Proceedings of FUELCELL2006
The 4th International Conference on FUEL CELL SCIENCE, ENGINEERING and TECHNOLOGY
June 19-21, 2006, Irvine, CA

FUELCELL2006-97067

MODELING AND SIMULATION OF A MODERN PEM FUEL CELL SYSTEM

Richard T. Meyer*and Bin Yao
Systems, Measurement, and Control
School of Mechanical Engineering
Purdue University
West Lafayette, IN 47907-1288
Email: rtmeyer@purdue.edu

ABSTRACT

Recent trends and advances in hydrogen/air Proton Exchange Membrane Fuel Cells (PEMFC) are incorporated into a dynamic control oriented model. This type of model is important for development of control systems for PEMFC powered transportation where unpredictable and widely varying changes in power demand can be expected. Self humidification and low pressure operation are the two major changes to past systems. As a result, a high pressure air compressor, air cooler, and inlet gas humidifiers are no longer required. Also, the likelihood of cathode flooding is reduced. The overall fuel cell model consists of four basic sub-models: anode, cathode, fuel cell body, and cooling. Additionally, the oxidant supply blower, cooling pump, and cooling fan are explicitly incorporated. Mass and energy conservation are applied to each using a lumped parameter control volume approach. Empirical modeling is minimized as much as possible, however it is necessary for model manageability in a control context. Interactions between each subsystem and balance of plant components are clearly defined. The overall model is capable of capturing the transient behavior of the flows, pressures, and temperatures as well as net output power. The influence of the charge double layer effect on transient performance is also explored. Numerical simulations of the system are presented which illustrate the usefulness of the model. Finally, future control work is described.

*Address all correspondence to this author.

NOMENCLATURE

A Area (cm^2, m^2)
c_n Fuel cell voltage equation constant
c_p Average specific heat at constant pressure (J/kg K)
c_v Average specific heat at constant volume (J/kg K)
C Equivalent capacitance of fuel cell body (F)
CS Control surface
CV Control volume
E Open circuit voltage (V)
E_{th} Thermal neutral reversible voltage (V)
f_n Pressure rise equation constant
h Specific enthalpy (J/kg)
h_c Convective heat transfer coefficient (W/m^2K)
i Current density (A/cm^2)
J Rotational inertia (kg m^2)
k Ratio of specific heats, c_p/c_v
K_F Nozzle flow efficiency coefficient
m Mass (kg)
M Molar mass (kg/gmol)
$\underline{n}$ Unit vector normal and away from control volume surface
N Number of
p Pressure (Pa)
Q Energy or heat produced (J)
R Resistance (Ohm)
T Temperature (K)
u Specific internal energy (J/kg K)
V Single fuel cell voltage (V)
$\underline{V}$ Velocity (m/s)
V_0 Activation polarization empirical constant

V_a Activation polarization empirical constant
V_i Voltage (V)
V_i Volume (m^3)
W Work (J)
Δ Difference
η Efficiency
λ Air stoichiometry ratio
ρ Material density (kg/m^3)
ϕ Relative humidity
Φ Flux Linkage (Vs/rad)
ω Angular velocity (rad/s)

Subscripts

act Activation
air Dry air
amb Ambient conditions
an Anode
ca Cathode
clt Coolant
co Crossover
dyn Dynamic
f Liquid fluid
fan Cooling fan
fc Fuel cell
fs Fuel supply
ha Humidified air
hex Heat exchanger
H_2 Hydrogen
H_2O Water
m Motor
mbr Membrane
N_2 Nitrogen
ohmic Resistance
os Oxidant supply
out Control volume outlet
O_2 Oxygen
pl Poles
pmp Pump
reg Regulator
rqs Rotor reference frame, stator q-axis
rx Reaction
s Stator
v Vapor
$\rightarrow$ To

INTRODUCTION

The PEMFC is a device that is able to produce electrical power via oxidation and reduction half reactions that are separated in space. Oxidation occurs at the anode, reduction at the cathode. In this case, the fuel and oxidant are hydrogen gas and air, respectively. There is no requirement that either the air or hydrogen be dry. The chemical reactions that occur:

$$Oxidation: \quad H_2 \rightarrow 2H^+ + 2e^- \tag{1}$$

$$Reduction: \quad \frac{1}{2}O_2 + 2e^- + 2H^+ \rightarrow H_2O \tag{2}$$

$$Overall: \quad H_2 + \frac{1}{2}O_2 \rightarrow H_2O \tag{3}$$

The overall fuel cell reaction is also known as the Faradic reaction. A cross section of a typical fuel cell is shown in Fig. 1. Individual cells are joined in series into stacks, anode to cathode bipolar plate, to increase the voltage output. Hydrogen enters the anode channels, permeates the gas diffusion layer and undergoes oxidation with the help of a catalyst that traditionally includes platinum. Electrons are then free for work while the hydrogen ions or protons travel through the proton exchange membrane. At the cathode, hydrogen ions, electrons, and oxygen from the air are combined by reduction into water, again with the help of a catalyst that typically contains platinum. The Faradic reaction product water and the remnants of the air are exhausted via the cathode channels. A charge can build up at the interfaces between the anode/membrane and cathode/membrane that behaves much like an electrical capacitor. This is known as the charge double layer. Performance of the fuel cell depends on many factors including the partial pressures of hydrogen and oxygen, temperature, and membrane humidity or water content. The complete PEMFC system has not only a fuel cell stack, but also fuel and oxidant supply devices, valves, and cooling components.

PEMFC systems have emerged as a possible replacement for internal combustion engines due to their efficiency, zero emission potential, and use of renewable fuels. Those used in transportation applications will experience unpredictable and widely varying power demand changes just like internal combustion engines in the majority of present vehicles. To satisfy the needs of dynamic performance, the PEMFC system will have to have a suitable control system able to manage its operation. However, before the design of any good control system there must also be a good control model to work from.

Models for control development attempt to capture the essence of the system dynamics in the simplest possible manner. Mechanistic models have been proposed that describe the fuel cell operation [1, 2] in great detail; however, often the equations can only be solved through numerical iteration and some

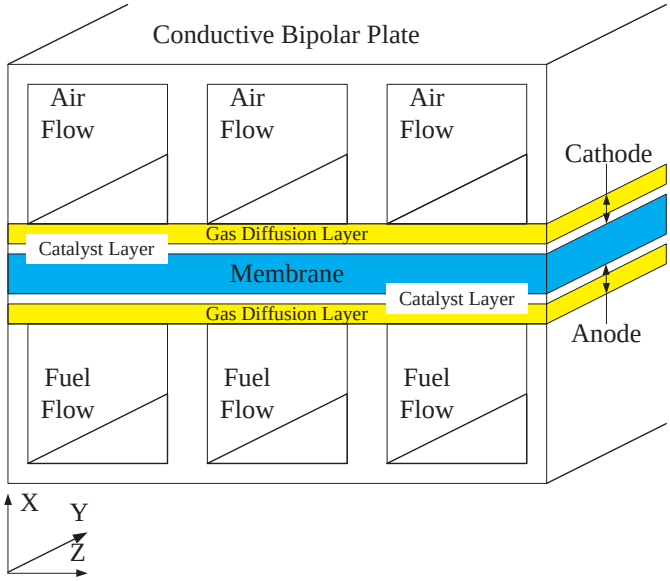

Figure 1. FUEL CELL CROSS SECTION

quantities that they require are not well established. An alternative to these is the zero dimensional models which are at most semi-empirical and involve fitting experimental fuel cell data to a phenomenological expression. This is used to create a polarization curve that shows the cell voltage versus current density at constant temperature and reactant partial pressures. Their advantage is that they are compact and do not require complex solution techniques. Many different expressions have been proposed and verified on actual systems or with data available in the open literature [3–12]. However, this only describes the fuel cell itself during operation. There is generally no provision for the ancillary devices and interactions that compose a complete system. Boettner et al. [13, 14] consider the power consumed by the fuel cell system components but neglect any dynamic interactions.

Pukrushpan et al. [15–17] developed a comprehensive dynamic model using a lumped parameter, control volume approach. An extensive fuel cell system was considered: air compressor, supply manifold, air cooler, reactant humidifiers, cathode channel volume, return manifold, anode channel volume, membrane humidification, and the fuel cell polarization curve. This formulation was primarily used to analyze the effect of sudden current changes on the air stoichiometry and net power developed. However, they assumed that the temperature was constant and uniform throughout the fuel cell body, anode volume, and cathode volume. Also, the fuel cell dynamic response due to the charge double layer was reasoned to not have an effect on the quantities of interest. The model was used by Gelfi et al. [18] to explore the use of an air blower in place of the air compressor. Results indicated that the low pressure blower system has marginally faster response to a commanded air flow input.

Xue et al. [19, 20] expanded upon the basic Pukrushpan et al. control volume approach by adding expressions for dynamic temperature response of the anode volume, cathode volume, and fuel cell body. Temperature has a great affect on the fuel cell performance. The temperature inside the anode or cathode volumes partly determines the partial pressure of a reactant as well as the partial and saturation pressures of water vapor. If the water partial pressure exceeds the vapor saturation pressure then liquid water can form, potentially degrading cell performance. The fuel cell body temperature also can have a significant effect. As body temperature rises so does the output voltage at a specific current density. They also include the charge double layer capacitance effect in the fuel cell response, believing it makes a difference in the system dynamics. The model is limited, with no consideration of the cooling system nor any of the other system components outside of the fuel cell. It also neglects any sort of reactant humidification.

Another aspect of a good model is its relevance. Typically, fuel cell system manufacturers are hesitant to release detailed information for fear of compromising their proprietary information. However, UTC Fuel Cells has developed a 250 kW bus known as ThunderPower and in 2005 published the system diagram in the open literature [21]. There are two important differences between it and the previous system analyzed by Pukrushpan et al.: an air blower instead of an air compressor and no external humidification equipment. Since there is no air compressor, the inlet air is not heated much above ambient, thus there is also no need for the associated air cooler as well. Also, the system lacks an external humidification system. Therefore, ambient air and dry hydrogen are being used to power the fuel cell. Research conducted into the construction and usage of self humidifying fuel cell membranes indicates that it is possible to operate with dry reactants, yet still retain similar performance to a normal membrane with fully humidified reactants [22–24]. The self humidification feature relies upon the amount of reactants that manage to permeate the membrane without undergoing the fuel cell or Faradic reaction. Crossover of reactants is a normal occurrence; therefore the self humidification feature takes advantage of material that would otherwise be wasted. There is also the additional benefit that crossover is reduced with self humidification. Watanabe et al. [22, 23] learned that self humidification leads to water entering the anode volume. The amount of water entering it is approximately the amount expected from the self humidification reaction. Meanwhile, the majority of the Faradic reaction product water enters the cathode volume. Self humidification can increase the back diffusion of water in the membrane which means that it is possible that an amount of the product water can instead travel to the anode rather than discharge into the cathode. The result is that the membrane can be considered completely and uniformly humidified. These hardware changes will affect the overall fuel cell model formulation.

The objective of the work presented here is to offer a modern and complete fuel cell system model that accounts for the major dynamics while remaining simple enough for future control development. Figure 2 shows the system proposed. The oxidant supply is an air blower and there is no air cooling or external reactant humidification. Naturally, the membrane is assumed to be self humidifying. Control volumes are utilized to capture the complex interaction of mass and temperature. The conservation of mass and energy are applied to each. Moreover, rotational dynamics are also considered. Mechanistic and empirical relations are used throughout the study. The complete model is implemented in the Matlab environment for presentation of simulation results. The model is fully capable of characterizing the transient response of a complete and modern fuel cell system.

MODEL DEVELOPMENT

A fixed control volume approach is used to analyze the fuel cell system dynamics. Control volume values, such as physical properties and states, are considered lumped quantities that are uniform across the entirety. This allows a lumped parameter analysis of the quantities of interest as they change over time. In this instance, the following assumptions are made about the control volumes.

1. All fluid velocities are low enough during operation that it is appropriate to ignore their kinetic energy.
2. Fluid particle velocity is zero everywhere on the inside surface of a control volume.
3. Any power transfer due to fluid stress is due to normal stress that occurs at the crossing of the control volume boundary.
4. Conservation of momentum can be ignored. Forces acting on the control volume, such as shear or body, are negligible.
5. All specific heats are constants equal to the average over a range of possible temperatures.
6. All pure gases and their mixtures are considered to obey the ideal gas law. Mixtures are non reacting and those with water vapor are considered to be single phase. Dry air has a volume that is 21% oxygen and 79% nitrogen.
7. Electrochemical reactions and fuel cell electrode electrical responses are so fast that their dynamics are ignorable.

The conservation of mass and energy are given respectively:

$$\frac{\partial}{\partial t}\int_{CV} \rho dV + \int_{CS} \rho(\underline{V}\cdot\underline{n})dA = 0 \tag{4}$$

$$\frac{\partial}{\partial t}\int_{CV} u\rho dV + \int_{CS} h\rho(\underline{V}\cdot\underline{n})dA = \dot{Q}_{net} + \dot{W}_{net} \tag{5}$$

Each of the control volumes represents a complex space in a simple manner, the model only regards volume. There are no provisions for variation of a parameter along a dimension or geometry changes in the volume. For example, the anode and cathode control volumes are simple summations of all of their respective flow channels and feed and discharge volumes without regard for geometry. However, lumped values can still provide adequate meaning. For example, Baschuk et al. [25] have shown that anode and cathode manifold and channel designs have a large impact on individual cells in a stack. Proper design results in an even distribution of properties across the stack. A lumped parameter approach can give meaningful results.

Self Humidification

Parameters for the self humidification mechanics described earlier are included in the model. However, the data in the literature is limited and inconsistent with regard to the amount of crossover gases lost as well as the water distribution. For example, values for the crossover hydrogen mass flow rate range from under 3% to nearly 20% of the Faradic reaction consumption at 1 A/cm^2 [22, 23]. Also, crossover and water quantities have only been referenced to the current density, with no regard for the effect of cell temperature. The hydrogen and oxygen crossover mass flow rates will be taken to be small compared to the Faradic consumption and allowed to go to zero. Similarly, the amount of water into the anode volume will be taken as zero while the amount of water entering the cathode volume will equal that produced by the Faradic reaction. When more pertinent literature becomes available, these terms can be given accurate meanings and evaluated for significance.

Anode Model

The anode volume supplies the fuel to the cell. The control volume is composed of all of the anode side flow channels and their feed and exit manifolds inside the fuel cell. It is assumed that hydrogen is stored at high pressure, 70 MPa [26], while a regulator makes it available to a metering valve at 1 MPa [27]. The hydrogen is taken to be at ambient temperature before the metering valve allows isentropic expansion into the anode volume. Hydrogen is let into the anode at a rate necessary to maintain the desired fuel pressure. Hydrogen is lost primarily through the oxidation half reaction but a small amount is also lost through membrane crossover. Any crossover fuel will be consumed in the self humidification reaction. Moreover, because of self humidification there can be passage of liquid water micro droplets to the anode channels [23]. This water can eventually be treated as vapor if the anode volume water partial pressure remains less than its saturation pressure. All of the water will remain in vapor

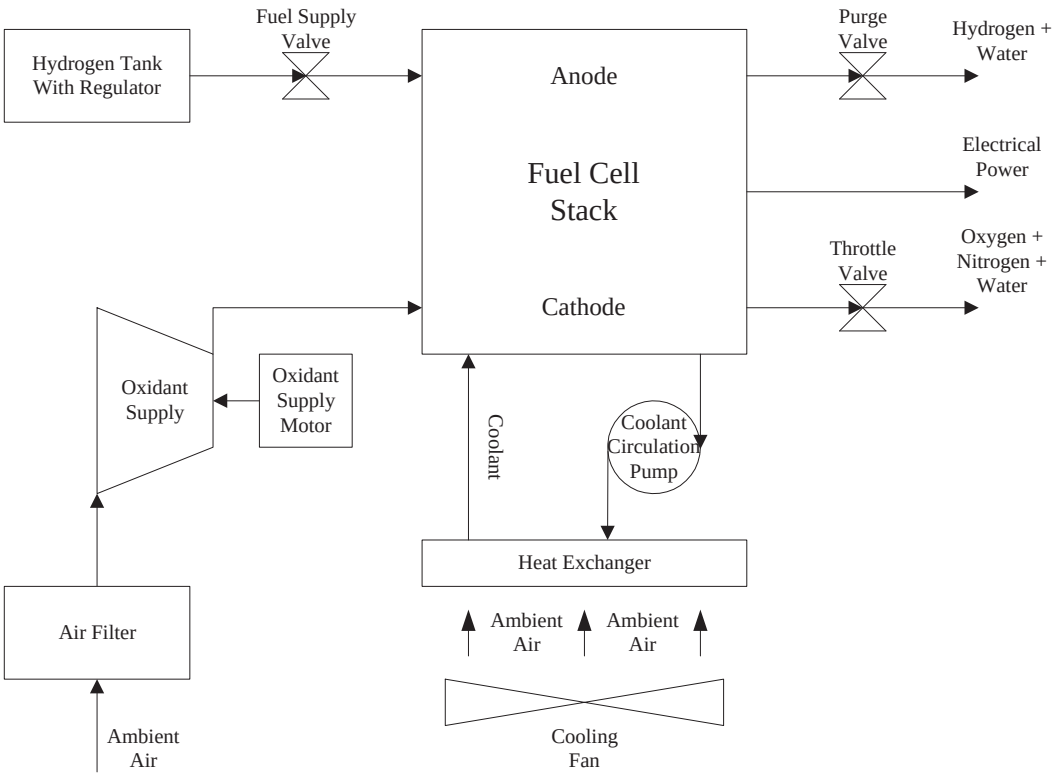

Figure 2. FUEL CELL BLOCK DIAGRAM

form until its partial pressure exceeds the saturation pressure at the anode volume temperature. During continuous operation this can occur unless the water vapor is removed in some manner. An option is the use of a purge valve; its use must be carefully managed to avoid fuel waste. A purge valve does not preclude the use of a powered fuel recirculation loop which some systems have to make sure that fuel is continuously and evenly distributed throughout the anode. The presence of a recirculation loop and pump will not affect the model formulation so long as they are taken to be perfectly insulated and any power used is insignificant in comparison to other parasitic devices. This model uses a purge valve without specific consideration of a circulation loop. The conservation of mass of hydrogen in the anode volume can be expressed as:

$$\frac{dm_{H_2,an}}{dt} = \dot{m}_{H_2,fs} - \dot{m}_{H_2,rx} - \dot{m}_{H_2,co} - \dot{m}_{H_2,purge} \tag{6}$$

Where:

$$\dot{m}_{H_2,rx} = \frac{M_{H_2} N_{fc} A_{mbr} i}{2F} \tag{7}$$

$$\dot{m}_{H_2,purge} = \frac{m_{H_2,an}}{(m_{H_2,an} + m_{H_2O,v,an})} \dot{m}_{purge} \tag{8}$$

Similarly, the water vapor mass is conserved.

$$\frac{dm_{H_2O,v,an}}{dt} = \dot{m}_{H_2O,mbr \rightarrow an} - \dot{m}_{H_2O,v,purge} \tag{9}$$

Where:

$$\dot{m}_{H_2O,v,purge} = \frac{m_{H_2O,v,an}}{(m_{H_2,an} + m_{H_2O,v,an})} \dot{m}_{purge} \tag{10}$$

Both the fuel supply and purge mass flow rates are control inputs. Valves used here are fast enough that their flow dynamics can be ignored. The mass flow through each valve can be found by treating it as a nozzle with performance dependent upon a

variable opening area and the pressure difference across it [28]. However, with the self humidification assumptions made, no water enters the anode and thus there is no need for purge usage. The fuel supply valve should be able to quickly meet any demands due to the order of magnitude pressure difference across it [17]. Therefore, simply commanding a fuel mass flow rate should be sufficient.

Energy is also conserved in the anode volume. Energy exits and enters via mass flow across the control volume. There is also convective heat transfer with the fuel cell body and evaporative cooling from the water exiting the membrane as a result of self humidification. The temperature of the fuel entering the anode is derived from isentropic gas expansion.

$$\begin{aligned}\frac{d}{dt}[(m_{H_2,an}+m_{H_2O,v,an})c_{v,an}T_{an}] =& \dot{m}_{H_2,fs}h_{H_2}(T_{fs}) \\ &- \dot{m}_{H_2,rx}h_{H_2}(T_{an}) \\ &- \dot{m}_{H_2,co}h_{H_2}(T_{an}) \\ &- \dot{m}_{H_2,purge}h_{H_2}(T_{an}) \\ &+ \dot{m}_{H_2O,mbr\rightarrow an}h_{f,H_2O}(T_{fc}) \\ &- \dot{m}_{H_2O,v,purge}h_{H_2O,v}(T_{an}) \\ &+ h_{c,an}A_{an}(T_{fc}-T_{an})\end{aligned} \tag{11}$$

Where:

$$T_{fs} = T_{H_2,reg}\left(\frac{p_{H_2,an}+p_{H_2O,v,an}}{p_{H_2,reg}}\right)^{\left(\frac{k_{H_2}-1}{k_{H_2}}\right)} \tag{12}$$

Cathode Model

The cathode volume is similar to the anode volume; it is the sum of cathode flow channels and feed and exit manifolds. Ambient air for the reduction reaction at the cathode is provided by an oxidant supply. In this case, it is a low pressure blower. Preceding the blower is an air filter whose pressure drop will be considered negligible. The air blower provides a certain mass flow rate of ambient air given its angular velocity and the pressure rise across it. It can be assumed that the rise is the difference between the cathode volume and ambient pressures if there is very little volume between the blower and cathode volume. The air exiting the blower has the same humidity ratio as the ambient air. Furthermore, the blower is powered by a brushless DC motor to prevent sparking and possible ignition of a fuel leak. Its electrical dynamics are considered sufficiently short to ignore. The blower model is based upon performance characteristic curves which plot both the flow parameter and overall efficiency versus the head parameter [28].

$$\dot{m}_{os} = f(\Delta p_{os}, \omega_{os}) \tag{13}$$

$$\eta_{os} = f(\dot{m}_{os}, \omega_{os}) \tag{14}$$

$$T_{os} = T_{amb} + \frac{T_{amb}\eta_{os,m}}{\eta_{os}}\left[\left(\frac{p_{ca}}{p_{amb}}\right)^{\frac{k_{air}-1}{k_{air}}} - 1\right] \tag{15}$$

The air required to meet the needed stoichiometry determines the desired output from the oxidant supply. Typically, stoichiometry is around two [29].

$$\dot{m}_{O_2,os} = \frac{\lambda N_{fc} A_{mbr} i M_{O_2}}{4F} \tag{16}$$

$$\dot{m}_{os} = (1+hr_{os})\frac{M_{air}}{(0.21)M_{O_2}}\dot{m}_{O_2,os} \tag{17}$$

The blower cannot instantly change its flow rate since rotational dynamics influence any required changes in speed. The dynamic response of the rotating system depends upon its inertia, the torque required, and torque contributed by the brushless DC motor. The motor torque is derived from a three phase balanced operation representation that has been linearized [30]. The control input to the blower is the stator voltage, $V_{rqs,os,m}$, in the motor torque relation.

$$\frac{d\omega_{os}}{dt} = \frac{1}{J_{os}}\left(\tau_{os,m} - \frac{\dot{W}_{os}\eta_{os,m}}{\omega_{os}}\right) \tag{18}$$

Where:

$$\dot{W}_{os} = \frac{\dot{m}_{os}\Delta p_{os}}{\eta_{os}\rho_{amb}} \tag{19}$$

$$\begin{aligned}\tau_{os,m} =& \eta_{os,m}\frac{3}{2}\left(\frac{N_{os,m,pl}}{2}\right)\left(\frac{\Phi_{os,m}}{R_{s,os,m}}\right) \\ &\cdot\left[V_{rqs,os,m} - \left(\frac{N_{os,m,pl}}{2}\right)\Phi_{os,m}\omega_{os}\right]\end{aligned} \tag{20}$$

The pressure ratio between the cathode volume and ambient is considered to be low enough with a blower that the oxidant supply total work can be calculated via an incompressible relationship. With a 10 kPa pressure rise, there is approximately 3% difference between the work calculated with incompressible and compressible methods.

The conservation of mass is applied to the cathode volume. Oxygen is consumed via the reduction reaction and a small amount is also lost to crossover. Nitrogen passes through without pause. Water vapor is added to that already present in the incoming air via micro droplets produced by the reaction. In a self-humidifying system the amount of water added to the cathode volume is equal to or less than that expected from the reaction. Naturally, water vapor is added to the air only if the vapor pressure inside the cathode is less than the partial pressure of the water. However, liquid water in the cathode seems unlikely; 100% humidified reactant air at 313 K that is heated to a typical operating temperature of 353 K has a relative humidity of only 16%. Of course, this value will be higher since there is an amount of reaction product entering that depends upon the current density and number of cells. It is possible that even the very dry conditions observed can be overcome if the gross power of the fuel cell stack is large enough. Flooding can be prevented by increasing the cathode volume temperature or pressure. The latter will result in an increased vapor exit mass flow rate. Only water in vapor form is considered here due to the capabilities of the system proposed. This results in the following relations for the oxygen, nitrogen and water vapor:

$$\frac{dm_{O_2,ca}}{dt} = \dot{m}_{O_2,os} - \dot{m}_{O_2,rx} - \dot{m}_{O_2,co} - \dot{m}_{O_2,out} \tag{21}$$

$$\frac{dm_{N_2,ca}}{dt} = \dot{m}_{N_2,os} - \dot{m}_{N_2,out} \tag{22}$$

$$\frac{dm_{H_2O,v,ca}}{dt} = \dot{m}_{H_2O,v,os} + \dot{m}_{H_2O,mbr\rightarrow ca} - \dot{m}_{H_2O,v,out} \tag{23}$$

Where:

$$\dot{m}_{O_2,rx} = \frac{M_{O_2} N_{fc} A_{mbr} i}{4F} \tag{24}$$

$$\dot{m}_{H_2O,mbr\rightarrow ca} = \frac{M_{H_2O} N_{fc} A_{mbr} i}{2F} \tag{25}$$

The cathode output mass flow rate is calculated using a nozzle relation [16, 17, 28, 31]. The pressure difference between the cathode and ambient drives the flow out of the cathode with the geometries of the stack and its exit acting as a virtual nozzle. The pressure ratio created with a blower is small enough that the critical pressure ratio can not be reached. The mixture exiting the cathode volume is discharged into the ambient.

$$\dot{m}_{O_2,out} = \frac{m_{O_2,ca}}{m_{O_2,ca} + m_{N_2,ca} + m_{H_2O,v,ca}} \dot{m}_{ca,out} \tag{26}$$

$$\dot{m}_{N_2,out} = \frac{m_{N_2,ca}}{m_{O_2,ca} + m_{N_2,ca} + m_{H_2O,v,ca}} \dot{m}_{ca,out} \tag{27}$$

$$\dot{m}_{H_2O,v,out} = \frac{m_{H_2O,v,ca}}{m_{O_2,ca} + m_{N_2,ca} + m_{H_2O,v,ca}} \dot{m}_{ca,out} \tag{28}$$

Where:

$$\dot{m}_{ca,out} = K_F A_{ca,out} \left\{ \frac{2 k_{air} \rho_{amb} p_{amb}}{k_{air} - 1} \left[\left(\frac{p_{amb}}{p_{ca}} \right)^{\frac{1-k_air}{k_{air}}} - 1 \right] \right\}^{0.5} \tag{29}$$

Cathode volume analysis also includes energy conservation. Similar to the anode, there is energy exchange via mass flow as well as convective heat transfer with the fuel cell body and evaporative cooling due to water entering the cathode.

$$\begin{aligned} \frac{d}{dt}[(m_{O_2,ca} + m_{N_2,ca} + m_{H_2O,v,ca}) c_{v,ca} T_{ca}] = \\ & \dot{m}_{O_2,os} h_{O_2}(T_{os}) \\ & - \dot{m}_{O_2,rx} h_{O_2}(T_{ca}) \\ & - \dot{m}_{O_2,co} h_{O_2}(T_{ca}) \\ & - \dot{m}_{O_2,out} h_{O_2}(T_{ca}) \\ & + \dot{m}_{N_2,os} h_{N_2}(T_{os}) \\ & - \dot{m}_{N_2,out} h_{N_2}(T_{ca}) \\ & + \dot{m}_{H_2O,v,os} h_{H_2O,v}(T_{os}) \\ & + \dot{m}_{H_2O,mbr\rightarrow ca} h_{f,H_2O}(T_{fc}) \\ & - \dot{m}_{H_2O,v,out} h_{H_2O,v}(T_{ca}) \\ & + h_{c,ca} A_{ca} (T_{fc} - T_{ca}) \end{aligned} \tag{30}$$

Cooling System Model

The cooling system is actually composed of four control volumes: sum of cooling channels and manifolds inside the fuel cell itself, heat exchanger (or radiator) coolant volume, heat exchanger cooling air volume, and the heat exchanger body. The

only direct interface with the fuel cell is through its cooling channels. The effort of the cooling system is directed at maintaining the input temperature of the coolant into these channels so that the desired stack temperature is held. The control inputs to the cooling system are the mass flow rates of the coolant and heat exchanger cooling air. The mass flow rate of the coolant through the system is assumed to be the same throughout. Similarly, the mass flow rate of the cooling air is assumed constant through the heat exchanger. These assumptions mean that the mass of coolant and air in their respective volumes is constant. Any heat transfer from the coolant pump to the coolant is considered negligible. This also holds for the cooling fan and cooling air. Finally, any coolant lines between the fuel cell and heat exchanger are assumed to be perfectly insulated so that there is no heat loss to the surroundings. With these assumptions, the four volumes can be modeled with the conservation of energy.

$$\begin{aligned} m_{clt,fc}c_{v,clt}\frac{dT_{clt,fc}}{dt} =& \dot{m}_{clt}h_{clt}(T_{clt,hex}) \\ &- \dot{m}_{clt}h_{clt}(T_{clt,fc}) \\ &+ h_{c,clt,fc}A_{clt,fc}(T_{fc} - T_{clt,fc}) \end{aligned} \tag{31}$$

$$\begin{aligned} m_{clt,hex}c_{v,clt}\frac{dT_{clt,hex}}{dt} =& \dot{m}_{clt}h_{clt}(T_{clt,fc}) \\ &- \dot{m}_{clt}h_{clt}(T_{clt,hex}) \\ &- h_{c,clt,hex}A_{clt,hex}(T_{clt,hex} - T_{hex}) \end{aligned} \tag{32}$$

$$\begin{aligned} m_{ha,hex}c_{v,ha,hex}\frac{dT_{ha,hex}}{dt} =& \dot{m}_{ha,hex}h_{ha}(T_{ha,in}) \\ &- \dot{m}_{ha,hex}h_{ha}(T_{ha,hex}) \\ &+ h_{c,ha,hex}A_{ha,hex}(T_{hex} - T_{ha,hex}) \end{aligned} \tag{33}$$

$$\begin{aligned} m_{hex}c_{v,hex}\frac{dT_{hex}}{dt} =& h_{c,clt,hex}A_{clt,hex}(T_{clt,hex} - T_{hex}) \\ &- h_{c,ha,hex}A_{ha,hex}(T_{hex} - T_{ha,hex}) \end{aligned} \tag{34}$$

Equation (31) describes the coolant in the fuel cell body while Eqns. (32)-(34) portray the coolant in the heat exchanger, cooling air in the heat exchanger, and the exchanger itself, respectively. $T_{ha,in}$ is taken to be the ambient air temperature. The heat exchanger body temperature is installed to act as a heat transfer conduit between the coolant and air streams. This is to negate the need for a heat exchanger effectiveness term.

The coolant pump and heat exchanger cooling fan are parasitic devices. To calculate the net power later on, their respective consumptions should be determined.

$$\dot{W}_{pmp,clt} = \frac{\dot{m}_{clt}\Delta p_{clt}}{\eta_{pmp,clt}\rho_{clt}} \tag{35}$$

$$\dot{W}_{fan,hex} = \frac{\dot{m}_{ha,hex}\Delta p_{ha}}{\eta_{fan,hex}\rho_{amb}} \tag{36}$$

The heat exchanger air cooling fan power is calculated with the incompressible fluid expression like the oxidant supply in the cathode. The ambient air pressure rise across the heat exchanger is assumed to be small enough that the incompressible relation is still valid. It should be pointed out that the rotational dynamics of these two flow devices are neglected unlike the oxidant supply. The rotational dynamics are much faster than those that govern the change in temperature. According to Guzzella [6] there is a two order of magnitude difference.

Furthermore, no matter how the power of the device is calculated, it does depend upon a pressure change. The pressure change depends upon the losses associated with the flow channel friction and geometry. By allowing the assumption that the flow is laminar as well, the change in pressure can be expressed with the following general loss equation.

$$\Delta p = f_1\left(\frac{\dot{m}}{\rho}\right) + f_2\left(\frac{\dot{m}}{\rho}\right)^2 \tag{37}$$

Fuel Cell Body Model

The fuel cell body is composed of the structure of the fuel cell itself. It encompasses the anode volume, cathode volume, and cooling channels. It is composed of the many bipolar and cooling plates, membranes, catalysts, gas diffusion layers, seals, etc. as well as the frame holds it all together. Mass conservation can be applied to it. However, it is assumed that mass transfer into and out of the diffusion layers is small compared to the total mass of the body. The conservation of energy is more relevant to the dynamic model since there is convective heat transfer between it and most of the other control volumes plus the ambient. Furthermore, the body is cooled by lower temperature gases that are consumed in the reaction and by any liquid water products leaving it. Finally, the Faradic reaction that generates power leads to internal heating of the body.

$$
\begin{aligned}
m_{fc}c_{v,fc}\frac{dT_{fc}}{dt} =& \dot{m}_{H_2,rx}c_{p,H_2}(T_{an}-T_{fc})+\dot{m}_{H_2,co}h_{H_2}(T_{an}) \\
&+\dot{m}_{O_2,rx}c_{p,O_2}(T_{ca}-T_{fc})+\dot{m}_{O_2,co}h_{O_2}(T_{ca}) \\
&-\dot{m}_{H_2O,mbr\rightarrow an}h_{f,H_2O}(T_{fc}) \\
&-\dot{m}_{H_2O,mbr\rightarrow ca}h_{f,H_2O}(T_{fc}) \\
&-h_{c,an}A_{an}(T_{fc}-T_{an})-h_{c,ca}A_{ca}(T_{fc}-T_{ca}) \\
&-h_{c,amb}A_{fc}(T_{fc}-T_{amb}) \\
&-h_{c,clt,fc}A_{clt,fc}(T_{fc}-T_{clt,fc}) \\
&+N_{fc}A_{mbr}i(E_{th}-V)
\end{aligned} \tag{38}
$$

E_{th} is the thermal neutral reversible voltage and in this case is equal to 1.48 V. It is the voltage expected from the higher heating value of the reaction, liquid water is the product rather than vapor. This takes into account the reversible and irreversible heat produced by the reaction [32]. The voltage term is calculated using a phenomenological equation developed by Pukrushpan et al. [15–17] and originally proposed by Guzzella [6]. The ohmic term has been modified. The original term relied on both membrane hydration and temperature. However, with self humidification the dependence on hydration has been removed. The terms are expanded further in Appendix A.

$$V = E - V_{act} - V_{ohmic} - V_{conc} \tag{39}$$

Where:

$$V_{act} = V_0 + V_a[1-\exp(-c_1 i)] \tag{40}$$

$$V_{ohmic} = i(c_{21}T_{fc}^2 + c_{22}T_{fc} + c_{23}) \tag{41}$$

$$V_{conc} = i\left(\frac{c_{31}i}{i_{lmt}}\right)^{c_{32}} \tag{42}$$

The advantage of this model over others is that it remains valid below the activation loss exchange current density. In transportation applications, the fuel cell system is not always operating near maximum power and may in fact be at idle, that is, simply supporting auxiliaries like air conditioning. The power draw is so low compared to the maximum that the desired current density is nearly zero. Moreover, the charge double layer adds a capacitance effect to the activation and concentration losses. If there is a sudden change in current, then the voltage will also change immediately due to the ohmic loss response; however, it may take some time to reach a steady state value due to the capacitance effect on the other two losses. The charge double layer dynamics can be modeled.

$$C\frac{dV_{dyn}}{dt} = A_{mbr}i\left(1-\frac{V_{dyn}}{V_{act}+V_{conc}}\right) \tag{43}$$

Therefore, the overall voltage equation must also be restated with the new dynamic voltage loss term.

$$V = E - V_{dyn} - V_{ohmic} \tag{44}$$

The net power currently delivered by the fuel cell system can now be formulated.

$$P_{net} = N_{fc}A_{mbr}iV - \dot{W}_{os} - \dot{W}_{pmp,clt} - \dot{W}_{fan,air} \tag{45}$$

SIMULATION RESULTS

The constant parameters used for the simulation are contained in Tables 1 and 2. The fuel cell system modeled can reach 73 kW gross power at 1.5 A/cm^2. The simulation is based on production components as much as possible. The oxidant supply or ambient air blower is a Phoenix Analysis & Design Technologies cathode air blower. Meanwhile, the coolant pumps are Ametek 26 gallon liquid devices. Deionized water is the coolant. Lastly, the heat exchanger cooling fans are Ebm-Papst Inc. W3G300EQW units. Appendices B-D contain specific modeling information for each. Part of the model is used to simulate the effect of the charge double layer. However, the complete model is used to simulate the system changing between different current density levels.

Charge Double Layer Dynamics

There has been disagreement in the past about the effect of the charge double layer capacitance on the fuel cell voltage response. Xue et al. [19, 20] believe that its effects are significant enough to include; meanwhile Pukrushpan et al. [17] maintain that it is negligible. Equations (39)-(44) are simulated with all other variables held constant except current density. No other dynamics are present. Required parameters other than those already listed are shown in Table 3. The current density is varied in step changes from 0.035 to 1.5 A/cm^2 and back again. The lower current density value represents an idle that consumes only 3 kW gross power. The current density span chosen is assumed to be the maximum possible during operation. Exploration of this difference should reveal the slowest voltage response encountered over the range of operation. Figure 3 displays the response to the current changes in both directions. The total fuel cell capacitance is 3 F during this simulation. Dynamics are more readily

Table 1. FUEL CELL SIMULATION PHYSICAL PARAMETERS

Parameter	Value	Source
A_{mbr}(cm^2)	280	[17]
C(F)	3	[29]**
E_{th}(V)	1.48	[29]
$h_{c,air,hex}A_{air,hex}$(W/K)	4700	[33]**
$h_{c,amb}A_{amb}$(W/K)	185.1	[34]**
$h_{c,an}A_{an}$(W/K)	131.4	[34]**
$h_{c,ca}A_{ca}$(W/K)	656.9	[34]**
$h_{c,clt,fc}A_{c,clt,fc}$(W/K)	28515	*
$h_{c,clt,hex}A_{c,clt,hex}$(W/K)	5445	[33]**
$K_fA_{ca,out}$(m^2)	1E-3	*
$m_{air,hex}$(kg)	0.04334	[35]***
$m_{clt,fc}$(kg)	5.1	*
$m_{clt,hex}$(kg)	11.5057	[35]***
m_{fc}(kg)	435	[34]**
m_{hex}(kg)	20.4	[35]***
N_{fc}	381	[17]
p_{amb}(Pa)	101325	*
T_{amb}(K)	288	*
V_{an}(m^3)	0.005	[17]
V_{ca}(m^3)	0.01	[17]
ϕ_{amb}	0.70	*
ρ_{amb}(kg/m^3)	1.2204	[36]
ρ_{clt}(kg/m^3)	971.72	[36]

* Design parameter

** Extrapolated from smaller fuel cell stack

*** Estimated

Table 2. FUEL CELL SIMULATION OPERATION CONSTANTS

Parameter	Value	Source
$p_{H_2,reg}$(Pa)	1E6	[27]
$T_{H_2,reg}$(K)	288	*
λ	2	[29]*

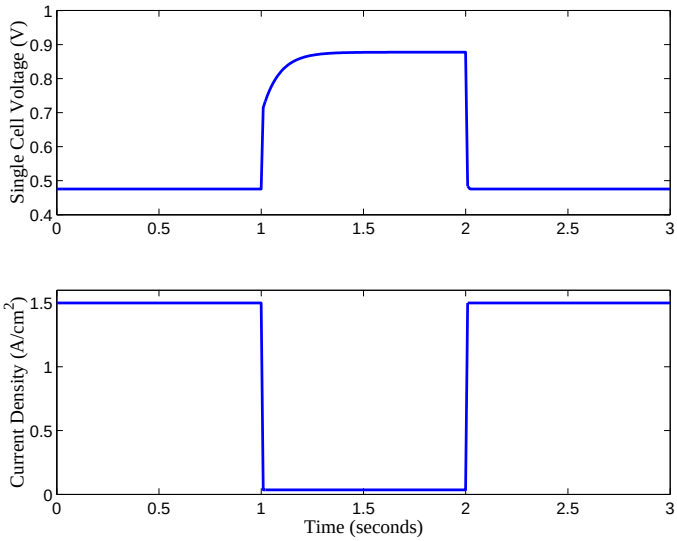

Figure 3. CHARGE DOUBLE LAYER EFFECT ON VOLTAGE

Table 3. CHARGE DOUBLE LAYER SIMULATION CONSTANTS

Constant	Value
p_{an}(Pa)	101325
p_{ca}(Pa)	101325
T_{fc}(K)	367
T_{ca}(K)	367
ϕ_{ca}	0

apparent during current rise, the 2% settling time is 0.2 seconds. The settling time is greater from low to high current since the effective resistance attributed to the activation and concentration losses increases by over 25 times. Naturally, from high to low current the effective resistance decreases by the same ratio. A 2% settling time of 1 second can be observed if the capacitance is increased to 15 F. This is a very high capacitance value [29]; therefore, it seems unlikely this value is realistic for an actual fuel cell stack. Regardless, the charge double layer capacitance should be considered during the selection of all pertinent dynamics. Simulation can reveal whether or not its effects are large enough to be included.

Fuel Cell System Dynamics

The complete model is implemented in the Matlab solution environment. The charge double layer dynamics are neglected due to their small effect on the overall system when the fuel cell body capacitance is 3 F. The equations are solved first at steady

Table 4. SYSTEM SIMULATION STEADY STATE VALUES

Parameter	$i = 0.5$ A/cm^2	$i = 1.0$ A/cm^2	$i = 1.5$ A/cm^2
$p_{H_2,an}$(Pa)	101325	101325	101325
$p_{O_2,ca}$(Pa)	9585	9761	10600
$p_{N_2,ca}$(Pa)	72117	73441	75686
$p_{H_2O,v,ca}$(Pa)	20241	20612	21242
T_{an}(K)	328	322	337
T_{ca}(K)	333	334	356
T_{fc}(K)	338	343	372
$T_{clt,fc}$(K)	337	341	367
$T_{clt,hex}$(K)	324	333	357
$T_{ha,hex}$(K)	313	303	307
T_{hex}(K)	319	319	334
ω_{os}(rad/s)	1094	2191	3294

state to show how system states can change between different current densities. Table 4 shows steady state operating information at current densities of 0.5, 1, and 1.5 A/cm^2. It is observed that the cathode relative humidity is one or below for all. The coolant and cooling air mass flow rates are chosen to maintain cathode relative humidity at one. If this requires rates that exceed their maximums, then the maximums are used. In this case, the relative humidity will always be less than one since the cathode volume vapor saturation pressure increases along with volume temperature.

Naturally, the model is meant for dynamic simulation. The first simulation steps the current from 0.6 to 1.5 A/cm^2, the second goes from 1.5 back down to 0.6 A/cm^2. In both cases, the simulation starts at steady state, but the time spent at the second current density is not long enough to return to steady state. However, the system response dynamics are still easily seen. The control inputs required to maintain the steady state current density levels without cathode flooding are shown in Tbl. 5. Moreover, anode and cathode control volume gas masses are not given, instead they are converted to partial pressure since that quantity is usually of more interest to fuel cell researchers.

The first simulation portrays a rise in current density from 0.6 to 1.5 A/cm^2 at 10 seconds. Figure 4 shows the response of the fuel cell partial pressures to this event. The hydrogen partial pressure initially drops but then begins to recover to its expected steady state value. The recovery is dependent upon the anode reaching its expected temperature during 1.5 A/cm^2 steady state operation since the control inputs are unchanging. The partial pressures of oxygen, nitrogen, and water vapor are initially

Table 5. DYNAMIC SIMULATION CONTROL INPUTS

Control Input	$i = 0.6$ A/cm^2	$i = 1.5$ A/cm^2
$\dot{m}_{air,hex}$(kg/s)	1.5066	6.5
$\dot{m}_{clt}$(kg/s)	0.6953	3
$\dot{m}_{H_2,fs}$(kg/s)	$6.6937 \cdot 10^{-4}$	$1.6734 \cdot 10^{-3}$
$\dot{m}_{purge}$(kg/s)	0	0
$V_{rqs,os,m}$(V)	57.9380	145.8878

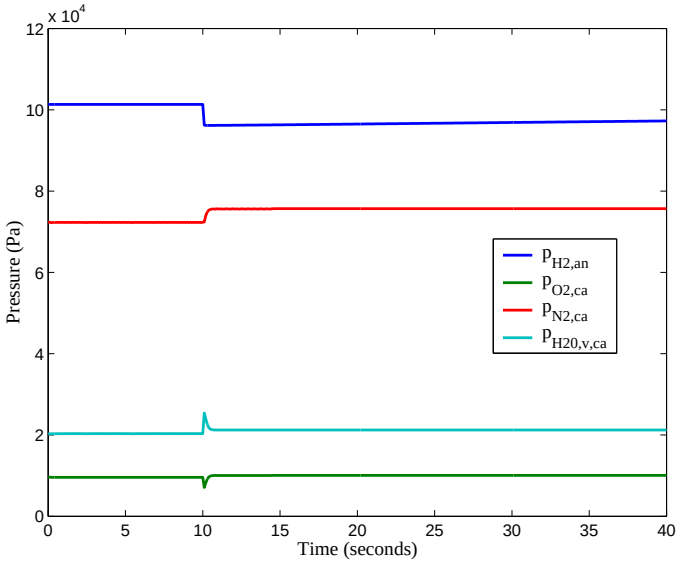

Figure 4. LOW TO HIGH CURRENT STEP AFFECT ON PRESSURE

dependent upon the angular velocity of the oxidant supply after the current density change. Figure 5 gives the response of the oxidant supply immediately after the current density change. The oxidant input cannot change instantly along with the current density. The oxygen partial pressure downward spike occurs because consumption has momentarily increased faster than the supply can provide. The water vapor partial pressure has an upward spike since its production momentarily overwhelms the removal capabilities of the cathode exit mass flow rate. The exit rate depends upon the cathode pressure which is determined by the oxidant supply. Both spikes last approximately as long as the oxidant supply takes to reach its final value. Nitrogen partial pressure has a smoother transition due to the fact that it it is not affected by a chemical reaction. The cathode partial pressures are near steady state at the end of the simulation; however, they do not reach it until the cathode temperature does also.

Figure 6 shows how the fuel cell system temperatures are

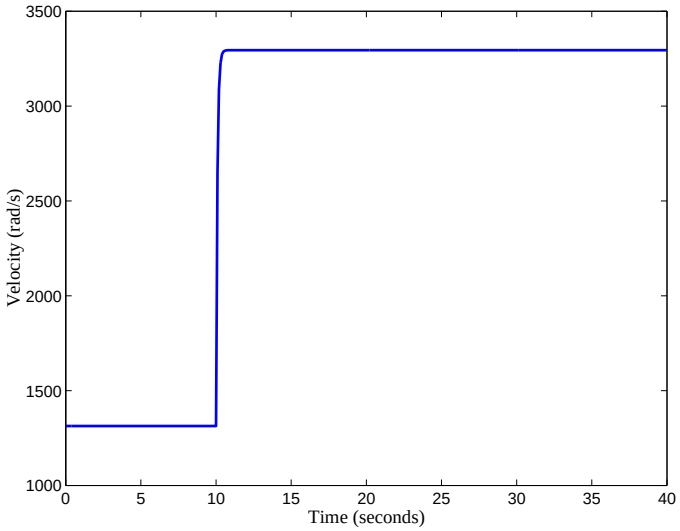

Figure 5. LOW TO HIGH CURRENT STEP AFFECT ON BLOWER SPEED

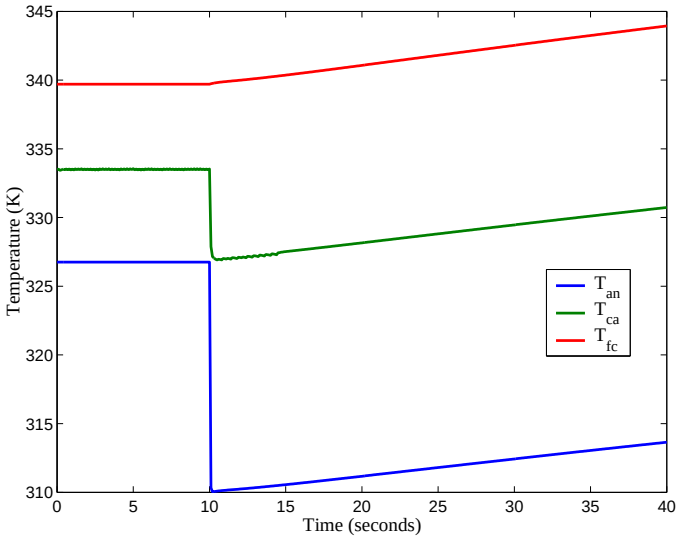

Figure 6. LOW TO HIGH CURRENT STEP AFFECT ON TEMPERATURES

affected when an increase in current density occurs. Unsurprisingly, the fuel cell body temperature begins rising immediately. Temperatures in the anode and cathode volumes experience a drop first and then begin rising. The initial drop is because that more, cooler reactants are being added which remove heat from the volumes.

The cooling system response in Fig. 7 displays the overall expected result such that all temperatures are trending upward at the end of the simulation. The coolant and cooling air mass flow rates immediately rise at the same time that more waste heat is produced in the cell. The fuel cell body thermal capacitance restricts how fast its temperature can rise. Therefore, the temperatures of the coolant in the fuel, humidified cooling air, and heat exchanger fall at first because of the greater flow rates. Meanwhile, the temperature of the coolant out of the heat exchanger actually rises. This is also due to the increased mass flow rates, they make it harder to remove heat from the coolant since it spends less time in the heat exchanger. The effect of thermal capacitance can also be seen in the initial response of all four temperatures. Increased thermal capacitance leads to smoother changes in the curve. Furthermore, there is an additional periodic nature to the humidified cooling air response which is due to its thermal capacitance. Increasing the mass of humidified air in the heat exchanger eliminates this part of its response.

The power generated and consumed by the fuel cell system is displayed in Figures 8 and 9. The net power continues to rise after the current density change, it does not immediately become the expected steady state value of 73 kW at 1.5 A/cm^2. The steady state fuel cell body temperature at 1.5 A/cm^2 is 372 K. The simulation ends before that temperature can be reached. The

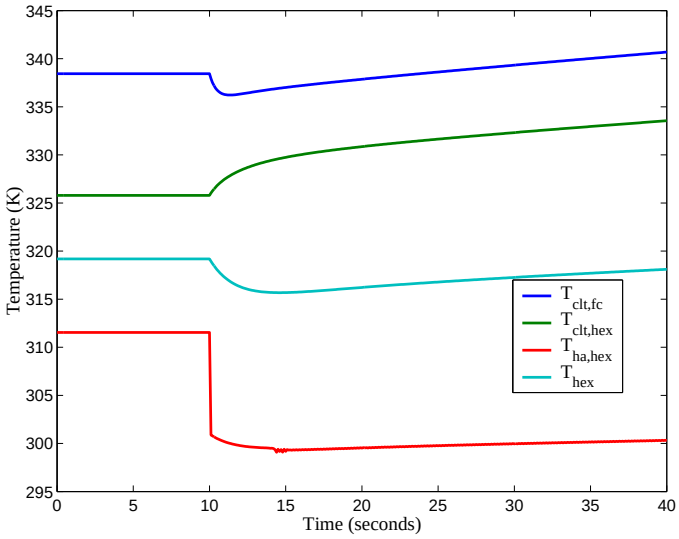

Figure 7. LOW TO HIGH CURRENT STEP AFFECT ON COOLING TEMPERATURES

gross power is the net power minus the parasitic losses. During the simulation, the oxidant supply, coolant pump, and cooling air fan power consumptions change as expected. The oxidant supply dynamics can also be seen in the power consumption curve shape immediately after the current change.

The second simulation is used to explore a step drop in current at 10 seconds. The current density decreases from 1.5 to 0.6 A/cm^2. The response trends described in the first simulation

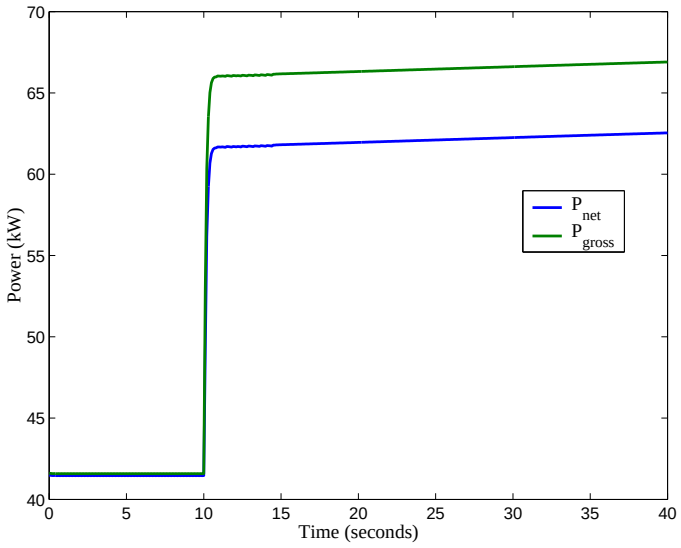

Figure 8. LOW TO HIGH CURRENT STEP AFFECT ON NET POWER

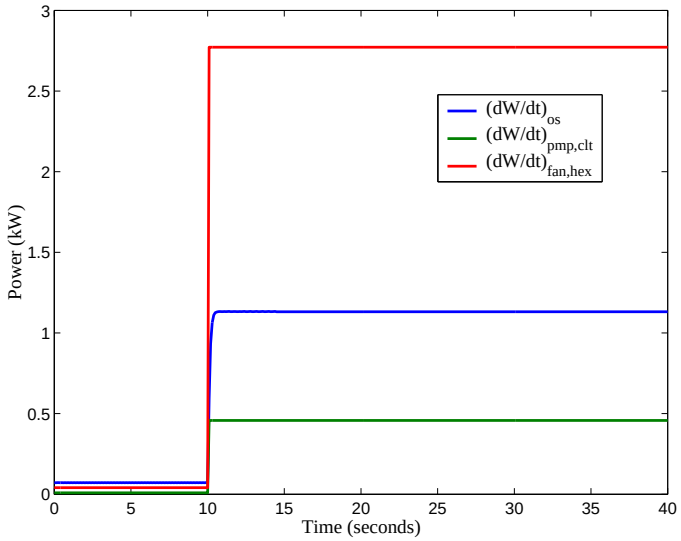

Figure 9. LOW TO HIGH CURRENT STEP AFFECT ON PARASITIC POWER

are the same except that where there is an increase there is now a decrease and vice versa. Figures 10-15 show the simulation responses. It is observed that the humidified cooling air temperature curve lacks the same periodic component that it had in the step current rise.

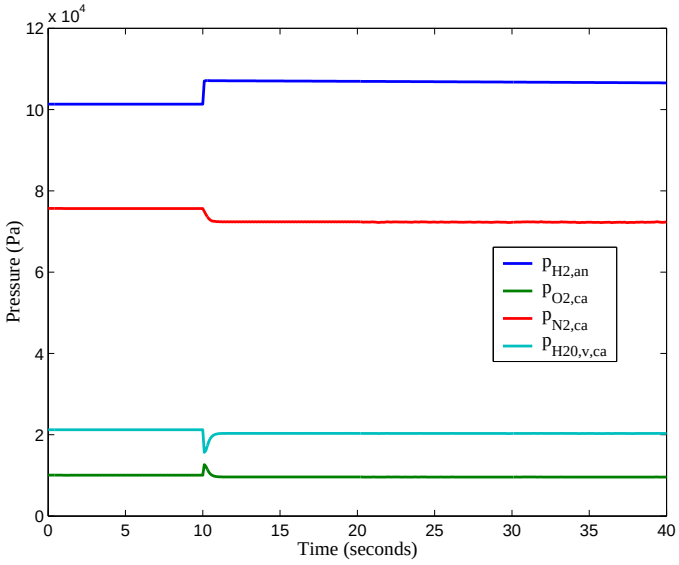

Figure 10. HIGH TO LOW CURRENT STEP AFFECT ON PRESSURE

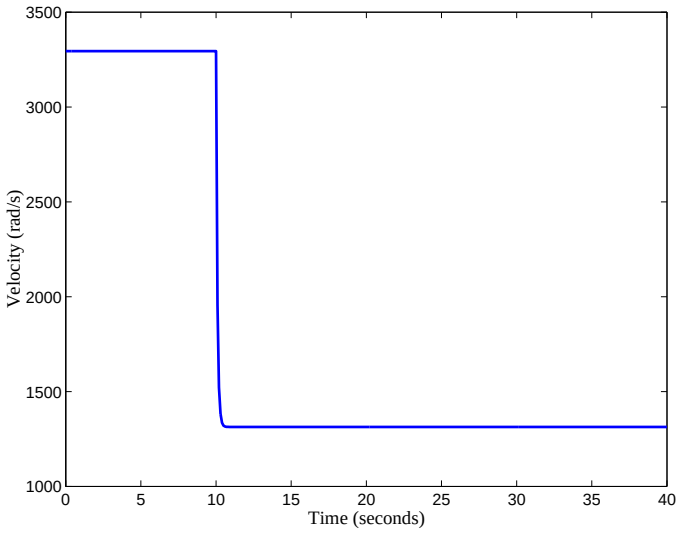

Figure 11. HIGH TO LOW CURRENT STEP AFFECT ON BLOWER SPEED

CONCLUSIONS

A comprehensive, zero dimensional, modern fuel cell system model has been presented. It incorporates recent improvements such as a low pressure oxidant supply and self humidification. The evolution of the necessity and form of the self humidification terms can occur once more detailed information becomes available in the literature. However, the model does consider all the other pertinent mass, temperature, and rotational dynamics in detail. This is an improvement over previous models

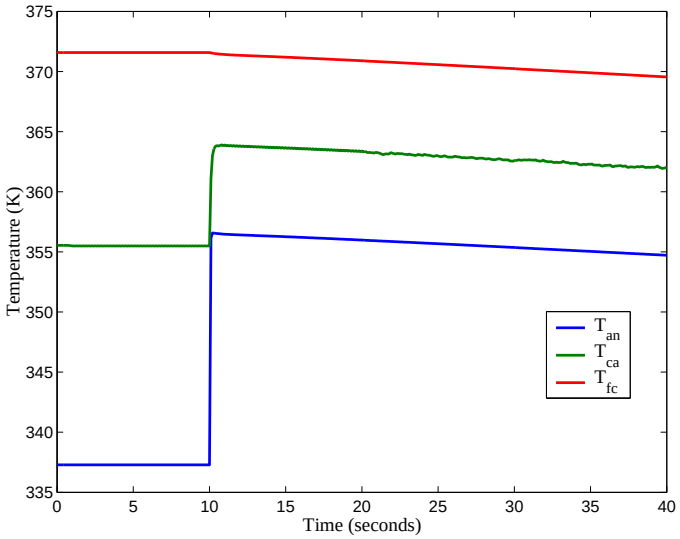

Figure 12. HIGH TO LOW CURRENT STEP AFFECT ON TEMPERATURES

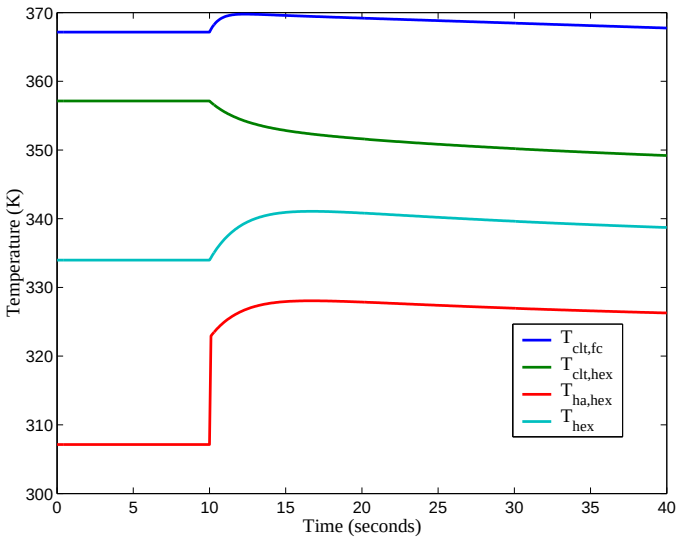

Figure 13. HIGH TO LOW CURRENT STEP AFFECT ON COOLING TEMPERATURES

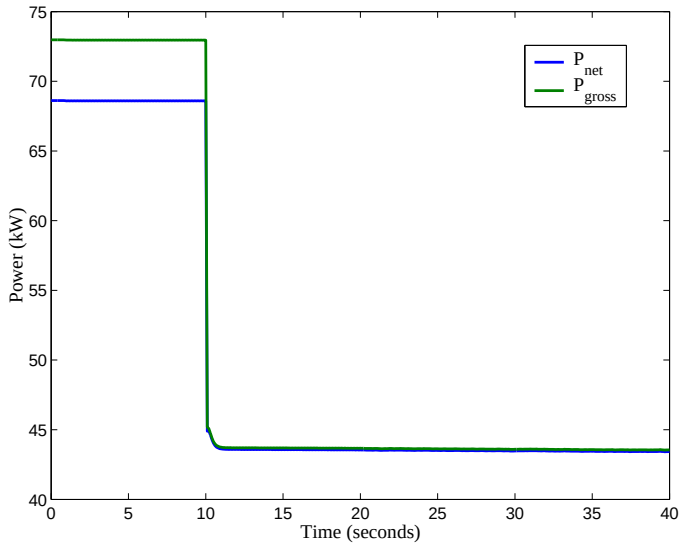

Figure 14. HIGH TO LOW CURRENT STEP AFFECT ON NET POWER

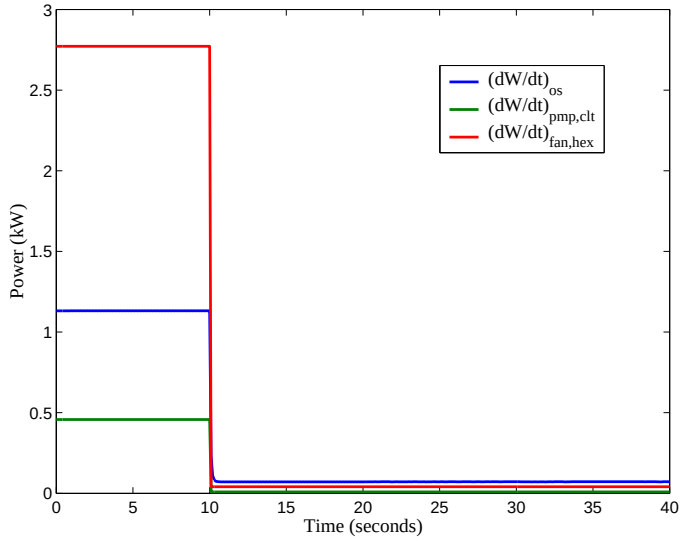

Figure 15. HIGH TO LOW CURRENT STEP AFFECT ON PARASITIC POWER

that have been proposed which remove the influence of temperature or balance of plant components. Simulation of the model gives expected responses, thus validating its general formulation. The physical parameters used in the simulation are drawn from a number of disparate sources thus the results should be recognized for their qualitative nature rather than specific values from an actual system.

The charge double layer dynamics are included in the model, but their effect depends upon the fuel cell capacitance value used. If the capacitance produces a 2% settling time smaller than the time scale of interest then its effect can be neglected. Anyone that includes this parameter in their model should check its behavior in isolation to ensure that their model is not made unnecessarily complex by a parameter that will have negligible bearing.

The simulation does show that temperature has a major affect on fuel cell gross power. After the current density step rise it is more than 6 kW less than can be expected at 1.5 A/cm^2 steady

state. It is not only until the fuel cell body reaches nearly 372 K that 73 kW is reached. The fuel and oxidant mass flow rates are already being held at their values needed for 73 kW output. This means that there is a need to manage the mass flow rates of the coolant and humidified cooling air. The use of temperature and mass flow rates together is necessary to achieve the maximum potential of the fuel cell system.

The model is simply formulated given the complexity and scope of it what it represents. It can be linearized rather easily for control work around a desired operating point. The objective of the control system is simple: provide the desired net power with minimum hydrogen usage. Naturally, this will depend upon intelligent management of the fuel supply, anode purge, oxidant supply, and temperatures. It will most likely not be an easy task; however this model is a first step toward this end.

ACKNOWLEDGMENT

Thanks go to the National Defense Science and Engineering Graduate Fellowship administered by the American Association of Engineering Education for supporting Richard Meyer.

REFERENCES

[1] Wang, C.-Y., 2004. "Fundamental models for Fuel Cell Engineering". *Chemical Reviews*(10), pp. 4727 – 4765.

[2] Yao, K., Koran, K., McAuley, K., Oosthuizen, P., Peppley, B., and Xie, T., 2004. "A Review of Mathematical Models for Hydrogen and Direct Methanol Polymer Electrolyte Membrane Fuel Cells". *Fuel Cells*(1-2), pp. 3 – 29.

[3] Amphlett, J., Baumert, R., Mann, R., Peppley, B., Roberge, P., and Harris, T., 1995. "Performance Modeling of the Ballard Mark IV Solid Polymer Electrolyte Fuel Cell I. Mechanistic model development". *Journal of the Electrochemical Society*(1), pp. 1 – 8.

[4] Amphlett, J., Baumert, R., Mann, R., Peppley, B., Roberge, P., and Harris, T., 1995. "Performance Modeling of the Ballard Mark IV Solid Polymer Electrolyte Fuel Cell II. Empirical model development". *Journal of the Electrochemical Society*(1), pp. 9 – 15.

[5] Kim, J., Lee, S.-M., Srinivasan, S., and Chamberlin, C. E., 1995. "Modeling of Proton Exchange Membrane Fuel Cell Performance with an Empirical Equation". *Journal of the Electrochemical Society*(8), pp. 2670 – 2674.

[6] Guzzella, L., 1999. "Control Oriented Modeling of Fuel Cell Based Vehicles". *Presentation at NSF Workshop on the Integration of Modeling and Control for Automotive Systems*, June.

[7] Squadrito, G., Maggio, G., Passalacqua, E., Lufrano, F., and Patti, A., 1999. "Empirical Equation for Polymer Electrolyte Fuel Cell (PEFC) Behaviour". *Journal of Applied Electrochemistry*(12), pp. 1449 – 1455.

[8] Mann, R. F., Amphlett, J. C., Hooper, M. A., Jensen, H. M., Peppley, B. A., and Roberge, P. R., 2000. "Development and Application of a Generalized Steady-State Electrochemical Model for a PEM Fuel Cell". *Journal of Power Sources*(1-2), pp. 173 – 180.

[9] Correa, J. M., Farret, F. A., and Canha, L. N., 2001. "An Analysis of the Dynamic Performance of Proton Exchange Membrane Fuel Cells Using an Electrochemical Model". *IECON Proceedings (Industrial Electronics Conference)*, pp. 141 – 146.

[10] Yerramalla, S., Davari, A., and Feliachi, A., 2002. "Dynamic Modeling and Analysis of Polymer Electrolyte Fuel Cell". *Proceedings of the IEEE Power Engineering Society Transmission and Distribution Conference*(SUMMER), pp. 82 – 86.

[11] Yerramalla, S., Davari, A., Feliachi, A., and Biswas, T., 2003. "Modeling and Simulation of the Dynamic Behavior of a Polymer Electrolyte Membrane Fuel Cell". *Journal of Power Sources*(1), pp. 104 – 113.

[12] Chiu, L.-Y., Diong, B., and Gemmen, R. S., 2004. "An Improved Small-Signal Model of the Dynamic Behavior of PEM Fuel Cells". *IEEE Transactions on Industry Applications*(4), pp. 970 – 977.

[13] Boettner, D. D., Paganelli, G., Guezennec, Y. G., Rizzoni, G., and Moran, M. J., 2001. "Proton Exchange Membrane (PEM) Fuel Cell System Model for Automotive Vehicle Simulation and Control". *American Society of Mechanical Engineers, Advanced Energy Systems Division (Publication) AES*, pp. 555 – 563.

[14] Boettner, D. D., Paganelli, G., Guezennec, Y. G., Rizzoni, G., and Moran, M. J., 2002. "Proton Exchange Membrane Fuel Cell System Model for Automotive Vehicle Simulation and Control". *Journal of Energy Resources Technology, Transactions of the ASME*(1), pp. 20 – 27.

[15] Pukrushpan, J. T., Stefanopoulou, A. G., and Peng, H., 2002. "Modeling and Control for PEM Fuel Cell Stack System". *Proceedings of the American Control Conference*, pp. 3117 – 3122.

[16] Pukrushpan, J. T., Peng, H., and Stefanopoulou, A. G., 2004. "Control-Oriented Modeling and Analysis for Automotive Fuel Cell Systems". *Journal of Dynamic Systems, Measurement and Control, Transactions of the ASME*(1), pp. 14 – 25.

[17] Pukrushpan, J. T., Stefanopoulou, A. G., and Peng, H., 2004. *Control of Fuel Cell Power Systems: Principles, Modeling, Analysis and Feedback Design*, 1st. ed. Advances in Industrial Control. Springer-Verlag Limited, London, England.

[18] Gelfi, S., Stefanopoulou, A. G., Pukrushpan, J. T., and Peng, H., 2003. "Dynamics of Low-Pressure and High-Pressure Fuel Cell Air Supply Systems". *Proceedings of the American Control Conference*, pp. 2049 – 2054.

[19] Xue, X., Tang, J., Smirnova, A., England, R., and Sammes, N., 2004. "System Level Lumped-Parameter Dynamic Modeling of PEM Fuel Cell". *Journal of Power Sources*(2), pp. 188 – 204.

[20] Pathapati, P., Xue, X., and Tang, J., 2005. "A New Dynamic Model for Predicting Transient Phenomena in a PEM Fuel Cell System". *Renewable Energy*(1), pp. 1 – 22.

[21] Narasimhamurthy, P., and Kabir, Z., 2005. "Overview of Field Performance of UTC Fuel Cells' Transportation Fuel-Cell Power Plants". *Proceedings of the 3rd International Conference on Fuel Cell Science, Engineering, and Technology, 2005*, pp. 633 – 640.

[22] Watanabe, M., Uchida, H., Seki, Y., Emori, M., and Stonehart, P., 1996. "Self-Humidifying Polymer Electrolyte Membranes for Fuel Cells". *Journal of the Electrochemical Society*(12), pp. 3847 – 3852.

[23] Watanabe, M., Uchida, H., and Emori, M., 1998. "Polymer Electrolyte Membranes Incorporated with Nanometer-Size Particles of Pt and/or Metal-Oxides: Experimental Analysis of the Self-Humidification and Suppression of Gas-Crossover in Fuel Cells". *Journal of Physical Chemistry B*(17), pp. 3129 – 3137.

[24] Liu, F., Yi, B., Xing, D., Yu, J., Hou, Z., and Fu, Y., 2003. "Development of Novel Self-Humidifying Composite Membranes for Fuel Cells". *Journal of Power Sources*(1), pp. 81 – 89.

[25] Baschuk, J., and Li, X., 2004. "Modelling of Polymer Electrolyte Membrane Fuel Cell Stacks Based on a Hydraulic Network Approach". *International Journal of Energy Research*(8), pp. 697 – 724.

[26] Quantum Technologies, 2005. TriShield Hydrogen Storage. URL `http://www.qtww.com/products/hydrogen_alt_fuel/hydrogen_storage`.

[27] Quantum Technologies, 2005. Regulators. URL `http://www.qtww.com/products/hydrogen_alt_fuel/regulators`.

[28] Thomas, P., 1999. *Simulation of Industrial Processes for Control Engineers*, 1st. ed. Butterworth-Heinemann, Oxford, England.

[29] Larminie, J., and Dicks, A., 2003. *Fuel Cell Systems Explained*, 2nd. ed. John Wiley & Sons Limited, West Sussex, England.

[30] Krause, P. C., and Wasynczuk, O., 1989. *Electromechanical Motion Devices*, 1st. ed. McGraw-Hill Book Company, New York, USA.

[31] Grujicic, M., Chittajallu, K., Law, E., and Pukrushpan, J., 2004. "Model-Based Control Strategies in the Dynamic Interaction of Air Supply and Fuel Cell". *Proceedings of the Institution of Mechanical Engineers, Part A: Journal of Power and Energy*(7), pp. 487 – 499.

[32] Baschuk, J., and Li, X., 2000. "Modelling of Polymer Plectrolyte Membrane Fuel Cells with Variable Degrees of Water Flooding". *Journal of Power Sources*(1-2), pp. 181 – 196.

[33] Zhang, Y., Ouyang, M., Lu, Q., Luo, J., and Li, X., 2004. "A Model Predicting Performance of Proton Exchange Membrane Fuel Cell Stack Thermal Systems". *Applied Thermal Engineering*(4), pp. 501 – 513.

[34] Amphlett, J., Mann, R., Peppley, B., Roberge, P., and Rodrigues, A., 1996. "Model Predicting Transient Responses of Proton Exchange Membrane Fuel Cells". *Journal of Power Sources*(1-2), pp. 183 – 188.

[35] Fluidyne, 2005. Race Winning Radiators-Racing Crossflow 2 Pass Radiators. URL `http://fluidyne.com/pl_radiators.html`.

[36] Moran, M. J., and Shapiro, H. N., 1988. *Fundamentals of Engineering Thermodynamics*, 1st. ed. John Wiley & Sons, Inc., New York, USA.

[37] Clark, T., and Arner, M., 2003. PEM Fuel Cell Blowers DOE Merit Review. Tech. rep., Department of Energy, May. URL `http://www.eere.energy.gov/hydrogenandfuelcells/pdfs/merit03/132_utfc_tom_clark.pdf`.

[38] Phoenix Design & Technologies, 2005. The PADT Turbomix. URL `http://www.padtinc.com/sales/fuelcell/turbomix/default.htm`.

[39] Ametek Technical & Industrial Products, 2005. 64 Frame Seal-Less Pump, 26 Gallon. URL `http://www.ametektmd.com/pdf/Pumps64-65.pdf`.

[40] Ebm-Papst Inc., 2005. W3G300EQ Specification Sheet. URL `http://www.ebmpapst.us/allpdfs/W3G300EQ.PDF`.

Appendix A: Fuel Cell Voltage Equation Terms

The model fitting parameters for the fuel cell voltage equation are derived from those given by Pukrushpan et al. [15–17]. They have been modified for a self humidifying membrane and performance equal to a a three fold pressure increase. The latter modification is based on the assumption that membranes are continuously improving. The Pukrushpan et al. expressions are based on fuel cell data from 1998. The equations require pressure to be converted to bars. Table 6 lists the constants.

$$\begin{aligned} E =& 1.229 - 8.5 \cdot 10^{-4}(T_{fc} - 298.15) \\ &+ 4.308 \cdot 10^{-5} T_{fc} \left[\ln\left(\frac{p_{H_2,an}}{p_{amb}}\right) + \frac{1}{2}\ln\left(\frac{p_{O_2,ca}}{p_{amb}}\right) \right] \end{aligned} \quad (46)$$

Table 6. FUEL CELL VOLTAGE EQUATION CONSTANTS

Constant	Value
c_1	10
c_{21}	$2.8383 \cdot 10^{-6}$
c_{22}	$-2.4216 \cdot 10^{-3}$
c_{23}	$6.5546 \cdot 10^{-1}$
c_{32}	2
i_{lmt}	2.2

Table 7. AIR BLOWER MODEL CONSTANTS

Constant	Value
J_{os}(kg/m^2)	$1.3 \cdot 10^{-3}$
$N_{os,m,pl}$	4
$R_{s,os,m}$(Ohm)	0.18
$\eta_{os,m}$	0.90
$\Phi_{os,m}$(Vs/rad)	0.022

$$\begin{aligned} V_0 =& 0.279 - 8.5 \cdot 10^{-4}(T_{fc} - 298.15) \\ &+ 4.308 \cdot 10^{-5} T_{fc} \left[\ln\left(\frac{3p_{ca} - \phi_{ca} p_{sat}(T_{ca})}{p_{amb}} \right) \right. \\ &\left. + \frac{1}{2} \ln\left(\frac{0.1173(3p_{ca} - \phi_{ca} p_{sat}(T_{ca}))}{p_{amb}} \right) \right] \end{aligned} \tag{47}$$

$$\begin{aligned} V_a =& (-1.618 \cdot 10^{-5} T_{fc} + 1.618 \cdot 10^{-2}) \left(\frac{3p_{O_2,ca}}{0.1173} + p_{sat}(T_{ca}) \right)^2 \\ &+ (1.8 \cdot 10^{-4} T_{fc} - 0.166) \left(\frac{3p_{O_2,ca}}{0.1173} + p_{sat}(T_{ca}) \right) \\ &- 5.8 \cdot 10^{-4} T_{fc} + 0.5736 \end{aligned} \tag{48}$$

$$c_{31} = \begin{cases} (7.16 \cdot 10^{-4} T_{fc} - 0.622) \cdot & \text{(49a)} \\ \left(\frac{3p_{O_2,ca}}{0.1173} + p_{sat}(T_{ca}) \right) & \\ -1.45 \cdot 10^{-3} T_{fc} + 1.68 \quad , \left(\frac{3p_{O_2,ca}}{0.1173} + p_{sat}(T_{ca}) \right) < 2 \text{ bar} & \\ (8.66 \cdot 10^{-5} T_{fc} - 0.068) \cdot & \text{(49b)} \\ \left(\frac{3p_{O_2,ca}}{0.1173} + p_{sat}(T_{ca}) \right) & \\ -1.6 \cdot 10^{-4} T_{fc} + 0.54 \quad ,\text{otherwise} & \end{cases}$$

$$\dot{m}_{os} = \begin{cases} \omega_{os}(-20.581 \left(\frac{p_{ca} - p_{amb}}{\omega_{os}^2} \right)^2 & \text{(50a)} \\ -1.4415 \cdot 10^{-3} \left(\frac{p_{ca} - p_{amb}}{\omega_{os^2}} \right) & \\ +4.1333 \cdot 10^{-5}) & \\ \quad , \left(\frac{p_{ca} - p_{amb}}{\omega_{os}^2} \right) \leq 9 \cdot 10^{-4} \text{ Pa s}^2/\text{rad}^2 & \\ \omega_{os}(-1.7973 \left(\frac{p_{ca} - p_{amb}}{\omega_{os}^2} \right) & \text{(50b)} \\ +1.6409 \cdot 10^{-3}) & \\ \quad ,\text{otherwise} & \end{cases}$$

$$\begin{aligned} \eta_{os} =& -2.8831 \cdot 10^{13} \left(\frac{\dot{m}_{os}}{\omega_{os}} \right)^3 + 9.5115 \cdot 10^{8} \left(\frac{\dot{m}_{os}}{\omega_{os}} \right)^2 \\ &+ 1.0387 \cdot 10^{4} \left(\frac{\dot{m}_{os}}{\omega_{os}} \right) + 0.17945 \end{aligned} \tag{51}$$

Appendix B: Air Blower Model

The Phoenix Analysis & Design Technologies cathode air blower [37, 38] can be modeled using characteristic curves that plot both the flow parameter and overall efficiency versus the head parameter. The model is estimated from their reported performance curves and device specifications.

Appendix C: Coolant Pump Model

The coolant pumps are Ametek $1.6 \cdot 10^{-3}$ m^3/s water circulators, each with a 24 volt brushless DC motor [39]. The pump is modeled with characteristic curves for the angular velocity as well as overall efficiency. The pressure drop across the coolant is found using Eqn. 37 with f_1 as $3.6607 \cdot 10^6$ and f_2 as $4.4148 \cdot 10^9$. A total of two coolant pumps in parallel are required to provide the maximum cooling rate of 3 kg/s. The flow rate used in the equations is the total and not the individual contribution from each flow device.

$$\omega_{pmp,clt} = 2.6211 \cdot 10^5 \left(\frac{\dot{m}_{clt}}{N_{pmp,clt} \rho_{clt}} \right) + 13.683 \tag{52}$$

$$\eta_{pmp,clt} = 1.3123 \cdot 10^{15} \left(\frac{\dot{m}_{clt}}{N_{pmp,clt} \rho_{clt} \omega_{pmp,clt}} \right)^3 - 4.9354 \cdot 10^{10} \left(\frac{\dot{m}_{clt}}{N_{pmp,clt} \rho_{clt} \omega_{pmp,clt}} \right)^2 + 2.6207 \cdot 10^{5} \left(\frac{\dot{m}_{clt}}{N_{pmp,clt} \rho_{clt} \omega_{pmp,clt}} \right) + 1.6444 \cdot 10^{-4} \quad (53)$$

Appendix D: Heat Exchanger Cooling Fan Model

The cooling fans are used to move waste heat from the heat exchanger into the ambient. The cooling fans are Ebm-Papst W3G300EQ series units [40]. The fans are modeled with characteristic curves for the rotational speed as well as overall efficiency. The pressure drop across the heat exchanger is found using Eqn. 37 with f_1 as $4.2856 \cdot 10^{-2}$ and f_2 as 6.9107. The maximum cooling air flow rate of 6.5 kg/s is provided by 12 fans in parallel. The flow rate used in the equations is the total and not the individual contribution from each flow device.

$$\omega_{fan,hex} = 6.6411 \cdot 10^{2} \left(\frac{\dot{m}_{ha,hex}}{N_{fan,hex} \rho_{amb}} \right) + 3.6640 \quad (54)$$

$$\eta_{fan,hex} = -1.0461 \cdot 10^{8} \left(\frac{\dot{m}_{ha,hex}}{N_{fan,hex} \rho_{amb} \omega_{fan,hex}} \right)^3 + 2.1049 \cdot 10^{5} \left(\frac{\dot{m}_{ha,hex}}{N_{fan,hex} \rho_{amb} \omega_{fan,hex}} \right)^2 + 1.3324 \cdot 10^{2} \left(\frac{\dot{m}_{ha,hex}}{N_{fan,hex} \rho_{amb} \omega_{fan,hex}} \right) + 6.0933 \cdot 10^{-2} \quad (55)$$